Journal of Applied Biology & Biotechnology 2026. Article in Press
Available online at http://www.jabonline.in
DOI: 10.7324/JABB.2026.248972

Phytochemical analysis and anti-breast cancer effects of *Terminalia bellirica* on MDA-MB-231 breast cancer cells: An integrated *in silico* and *in vitro* studies

Aishwarya Gadade[1], Laxmi Pattanashetti[2], DSNBK Prasanth[3], Sangameshwar G. Halkavatagi[2], Zabin K. Bagewadi[1], Deepak A. Yaraguppi[1]*, Nidhi S Hallikeri[1]

[1]Department of Biotechnology, KLE Technological University, Hubballi, Karnataka, India.
[2]Department of Pharmacology, KLE College of Pharmacy, Hubballi, KLE Academy of Higher Education and Research, Belagavi, Karnataka, India.
[3]School of Pharmacy & Technology Management, SVKM's Narsee Monjee Institute of Management Studies (NMIMS), Polepally SEZ, TSIIC, Jadcherla, Mahbubnagar, India.

ARTICLE INFO

Article history:
Received on: 24/03/2025
Accepted on: 26/12/2025
Available online: ***

Key words:
Terminalia bellirica,
Anti-breast cancer,
Liquid chromatography mass spectrometry, Network pharmacology, Molecular docking, Molecular simulations, MTT assay.

ABSTRACT

Terminalia bellirica, a traditional medicinal plant, has been studied for its possible anti-breast cancer activity via an integrated *in silico* and *in vitro* approach. Phytochemical profiling via liquid chromatography-mass spectrometry yielded a total of 13 bioactive compound candidates, 7 of which presented favorable drug-likeness scores. *In silico* toxicological and absorption, distribution, metabolism, and excretion (ADME) profiling further strengthened the therapeutic potential and safety of these compounds. Network pharmacology offered insight into several key targets associated with breast cancer, such as ERBB2, Akt1, MAPK1, EGFR, VEGFA, and ESR1, whereas enriched signaling pathways included the PI3K-Akt, MAPK, and HIF-1 pathways. Molecular docking and dynamics simulations have revealed strong and stable binding interactions between 6-Prenylnaringenin and its respective target, the kinase domain of human HER2 (erbB2). Hydroalcoholic extracts from *T. bellirica* seeds were also shown *in vitro* to have cytotoxic effects on Anderson Cancer Center (MDA) and metastatic breast (MB) (MDA-MB)-231 breast cancer cells, with a half maximal inhibitory concentration value of 57.83 µg/mL determined via the which is chemically 3-(4,5-dimethylthiazol-2-yl)-2,5-diphenyltetrazolium bromide (MTT) assay. These findings suggest the promising anti-breast cancer potential of *T. bellirica* and its phytocompounds and offer a basis for further pre-clinical and clinical investigations.

1. INTRODUCTION

The use of *Terminalia bellirica* dates back thousands of years, and this herb has been in high demand among traditional medicine practitioners worldwide [1]. *T. bellirica* (Beleric) is a tropical fruit with a high level of bioactive compounds of pharmaceutical value [2]. Its antibacterial, antioxidant, and anticancer effects have been established recently, which has further established its universal applicability as a natural pharmacological source. Negligible literature had been reported on the cytotoxic or anticancer effects of the hydroalcoholic seed extracts of the plant, especially against breast cancer cell lines, although its antioxidant, antimicrobial, and anti-inflammatory properties had been extensively investigated [3]. Here, liquid chromatography-mass spectrometry (LC-MS)-based phytochemical profiling and Soxhlet-induced seed extraction techniques were used in the analysis of bioactive constituents [4], which were later predicted and evaluated with reference to drug-likeness in order to gain insight into the therapeutic value of the bioactive compounds.

T. bellirica harbors a number of effective antioxidant molecules, including polyphenols, tannins (gallic acid, ellagic acid, and chebulic acid), flavonoids, and gallotannins that exhibited high free radical scavenging properties in both DPPH and FRAP assays [5]. These compounds induced cellular antioxidant pathways (e.g., Nrf2, MAPK/NF-kB, and Akt/AMPK) and played a role in hepatoprotective, anti-inflammatory, and antidiabetic functions. The antimicrobial activity also had a broad spectrum of the plant extracts, with the methanolic and aqueous fruit extracts exhibiting significant inhibition zones and low MIC values against pathogenic bacteria, including drug-resistant strains such as MRSA, ESBL-producing *Escherichia coli*, and multidrug-resistant *Pseudomonas aeruginosa* [6]. Moreover, the *T. bellirica* extracts showed selective cytotoxicity to liver (HepG2) and lung (A549) carcinoma cell lines; tumor growth was inhibited by tannin-containing fractions, which regulated ERBB, PI3K-Akt, and MAPK pathways [7]. Cisplatin and doxorubicin (synergetic effect) were also reported with CI < 1 and low toxicity to normal cell lines [8].

*Corresponding Author:
Deepak A. Yaraguppi,
Department of Biotechnology, KLE Technological University, Hubballi, Karnataka, India. E-mail: deepak.yaraguppi@kletech.ac.in

Despite the documented cytotoxicity of *T. bellirica* fruit extracts, the anticancer activity of its hydroalcoholic seed extracts against the aggressive triple-negative MDA-MB-231 breast cancer cell line has not been well studied. Moreover, a comprehensive integration of *in silico* approaches, such as network pharmacology and molecular dynamics (MD), to identify the bioactive compounds and their mechanisms of action has been lacking. Therefore, this study proposed that the hydroalcoholic seed extract of *T. bellirica* had an anti-breast cancer effect on MDA-MB-231 cells through specific phytocompounds that target oncogenic signaling pathways. This was tested through LC-MS profiling, computational modeling, and *in vitro* validation using MTT assay. Considering the difficulty of phytochemical interactions in cancer biology, an *in silico* model provided a rational method to predict and analyze molecular interactions between bioactive compounds and cancer-associated targets. This aided in identifying the most promising candidates for further validation through *in vitro* studies. An *in silico* approach incorporated the evaluation of ADME properties as well as drug-likeness and toxicological profiles of the identified phytocompounds [9,10]. This was followed by molecular docking studies to examine the binding affinities of compounds against different target proteins involved in breast cancer. Further evaluation of ligand-receptor interactions was performed using MD simulations [11]. Herein, a fastidious experimental and computational pipeline was presented to screen conceivable bioactive candidates from *T. bellirica* for possible anti-breast cancer therapeutics. The MTT (3-(4,5-dimethylthiazol-2-yl)-2,5-diphenyltetrazolium bromide) bioassay, which assesses cell viability, confirmed this bioactivity. The present study aimed to evaluate the anticancer potential of hydroalcoholic extracts of *T. bellirica* seeds against breast cancer cells and to elucidate their molecular mechanisms through an integrated *in silico* approach. It was hypothesized that the *T. bellirica* seed extract showed anticancer activity against breast cancer through *in silico* studies by interacting with the key target protein, and this was further proved by MTT assay. The objectives of this work were to prepare and characterize the hydroalcoholic extract of *T. bellirica* seeds, to identify and evaluate active compounds through *in silico* approaches targeting key breast cancer proteins, and finally to assess its activity against breast cancer cell lines.

2. MATERIALS AND METHODOLOGY

2.1. Seed Collection and Extraction

Seeds of *T. bellirica*, a very important medicinal tree of the *Combretaceae* family, were collected from Yuvika Herbs. All these seeds were thoroughly inspected for their morphological characteristics, such as shape, size, and texture, as per standard identification protocols of botany [12]. The study seed was identified and authenticated by Dr. K. Madhava Chetty, from the Department of Botany, Sri Venkateswara University, Tirupati, India. The collected seeds were thoroughly cleaned, dried, and stored in controlled conditions to maintain seed viability and homogeneity for future studies [13].

Seeds of *T. bellirica* were obtained, authenticated, and processed for extraction. A modified Soxhlet extraction method employing organic solvents was considered best for maximum phytocompound extraction [14,15]. The extraction of *T. bellirica* seeds was carried out with 100% ethanol. Three hundred milliliters of the solvent were used to extract 15 g of strictly suspended *T. bellirica* seed powder. A Soxhlet apparatus was used for extraction for up to 3 h, until the solvent in the extractor siphon tube becomes colorless. The temperature was initially maintained at 30°C as the solvent started to boil, with a gradual increase in temperature to 70°C without exceeding the boiling point. The extract was concentrated at 45°C while a rotary evaporator was used for 45 min and lyophilized, and the dry crude concentrate was stored at −4°C for *in vitro* anticancer activity and LC–MS data analysis [16].

2.2. LC–MS Analysis

LC–MS analysis of *T. bellirica* was conducted on a Waters 2645 separation module with a Waters Micromass ZQ mass spectrometer. The mobile phases consisted of 0.1% formic acid in water (Mobile Phase A) and 0.1% formic acid in acetonitrile (Mobile Phase B). Sample preparation consisted of the solubilization of 20 mg of the dry powder in methanol, followed by adjusting the final volume to 25 mL, followed by filtration with a 0.22 µm syringe filter to remove particulates. Analysis had a 10 µL injection volume. The gradient program proceeded as follows: The initial flow of 0.500 mL/min with 90% Mobile Phase-A, along with 10% Mobile Phase B, was switched to 5% Mobile Phase A and 95% Mobile Phase-B at 7.00 min, remaining the same until 12.00 min. The flow switched back to the initial conditions by 13.00 min and remained the same until the end of the run at 15.00 min. The column was an Accucore C18 (50 × 4.6 mm, particle size of 5 µm) from the company Thermo Scientific, maintained at 40°C. The mass spectrometer operated under positive electrospray ionization (ES+) conditions with the capillary voltage set as 2.8 kV, the cone voltage as 30 V, the source temperature as 140°C, as well as the desolvation temperature as 400°C, with the desolvation gas set at 600 L/h. Full scan data were acquired over the mass range of m/z 100–1000. Data processing occurred with the use of the MassLynx V4.1 software that can permit detailed examination of the resultant mass spectra.

The work starts with the selection of phytocompounds to be used as inferences from an LC–MS analysis of the samples. All of these compounds were obtained from a formatted library of plant-derived metabolites. The molecular specifications of the compounds, for example, using ChemDraw and MolSoft (MolSoft Drug Likeness and Molecular Properties Software), were determined through computational tools and software incorporated into the study. The molecular formula, molecular weight, HBA, HBD, MolLogP, MolLogS, molecular polar surface area (MolPSA), and molecular volume (MolVol) were calculated through standard algorithms integrated into these software platforms. The pKa values of the basic and acidic groups were predicted through MarvinSketch, and blood–brain barrier (BBB) penetration scores were derived through the brain or intestinal estimated permeation (BOILED-Egg) model.

The MolSoft drug-likeness scoring function judges each of these compounds with respect to the drug-likeness properties because the function describes the compatibility of molecular properties with respect to standard pharmacokinetic and pharmacodynamic profiles. Positive scores indicate an increased chance for that compound to be a drug candidate [17,18].

To strengthen its accuracy and replicability, measurements were made in triplicate for every single observation, and the results were considered using simple statistical methods. Positive drug-likeness scores were used to study other pharmacological aspects of these compounds in terms of the overall balance between hydrophilicity, lipophilicity, and other parameters that seem very important.

2.3. Toxicological Properties of the Phytocompounds

The ProTox-II database was used for the online *in silico* prediction of the toxicological effects of 13 phytocompounds. An assessment

of the toxicological effects of the phytocompounds, such as their carcinogenicity, immunotoxicity, mutagenicity, and cytotoxicity, was performed [19]. The ProTox-II database utilizes machine learning models to predict toxicity profiles, providing insight into possible undesirable effects. The results for each compound were recorded systematically, and the data were further analyzed to identify any patterns or correlations between the phytocompounds and their toxicological profiles.

2.4. ADME Properties of the Phytocompounds

Each compound's ADME properties were calculated through the Swiss ADME database. The ADME properties of the phytochemicals were evaluated to assess their drug-likeness and pharmacokinetic potential. Parameters such as gastrointestinal absorption, BBB permeability, P-glycoprotein substrate, and the major cytochrome P450 inhibitors CYP1A2, CYP2C19, CYP2C9, CYP2D6, and CYP3A4 were assessed [20]. Drug likeness was derived from Lipinski's rule of five, with the number of rule violations noted for each. The analysis was carried out using validated *in silico* tools and databases. GI absorption and BBB permeability were used to assess bioavailability and central nervous system penetration, whereas Pgp substrate and CYP enzyme inhibition data would have added to the knowledge of possible interactions and metabolic stability. The data were organized systematically to indicate the extent of adherence of each compound to Lipinski's rule.

2.5. Target Identification

Canonical SMILESs were analyzed for target prediction through Swiss Target Prediction (http://swisstargetprediction.ch/), aligning them with known therapeutic drug molecules [21]. To ensure the robustness of the network and avoid spurious links, clear thresholds were applied for target inclusion. For the phytocompounds, targets were predicted through Swiss Target Prediction, and only those with a probability score >0.1 were retained. In addition, target proteins associated with breast cancer were identified on the basis of documented targets sourced from the GeneCards Database (https://www.genecards.org/). For breast cancer-associated targets from the GeneCards database, a relevance score threshold of >10 was applied, focusing the analysis on the top 1842 high-confidence genes. To identify combined genes, compound-related genes and disease-related genes were merged, and the overlap was visualized through a Venn diagram [18].

2.6. Pathway and Network Analysis

The STRING database (https://string-db.org/) and the Kyoto Encyclopedia of Genes and Genomes (KEGG) pathway database (https://www.genome.jp/kegg/) were used to investigate protein–protein interactions (PPIs) and molecular pathways associated with protein targets related to BC [22]. The relationships among compounds, target proteins, and pathways relevant to breast cancer were visualized through Cytoscape v3.6.1 (https://cytoscape.org/) [23]. Network visualization was enhanced by employing a color scale and varying node sizes, where the size of each node corresponded to its edge count (number of connections). Nodes with higher edge counts were represented as larger nodes, highlighting their significance in the network.

2.7. Molecular Docking

The present investigation employed the molecular docking of ligands against the target protein through AutoDock Vina. First, Open Babel software was employed to generate the three-dimensional structures of the ligands for docking after they were obtained through PubChem. Preparations for docking were also conducted for the receptor, the target protein. The grid box for docking was centered on the centroid of the co-crystallized ligand (coordinates: x = 26.5, y = 20.8, z = 49.1) with dimensions set to 60 × 60 × 60 Å. The exhaustiveness was set to 32. All other parameters were kept at their default values. Furthermore, duplicate docking procedures were initiated. The binding affinities of the resulting docking locations were assessed, and the optimal poses were selected for further analysis. The PyMOL algorithm was utilized to analyze the ligand-receptor interactions and binding mechanism. The efficacy of the medicines and phytochemicals as inhibitors of the target protein was evaluated by docking analysis [24].

2.8. MD

The MD simulations were conducted on the kinase domain structure of human HER2, the ErbB2 protein (PDB ID: 3PP0), in complex with ligands of first interest obtained from the docking investigations. The ligand topologies were prepared with the ATB server. The GROMACS pdb2gmx module added hydrogen atoms to the molecules, as well as generated the protein topologies with the CHARMM36 force field. The systems prepared were initially energy-minimized in a vacuum with the steepest descent algorithm over 50,000 steps to remove steric clashes. The systems were then solvated in a cubic periodic box with at least 1.0 nm distance between the protein and the box edge using the simple point charge water model. The proper quantities of Na^+ and Cl^- counterions were introduced to neutralize the system as well as to give a physiological salt concentration of 0.15 M [25]. The systems were equilibrated over two stages: Initially, under an NVT (constant number of particles, volume, and temperature) ensemble for 100 ps at 300 K with the v-rescale thermostat, followed by one NPT (constant number of particles, pressure, and temperature) ensemble for 100 ps at 1 bar with the Parrinello–Rahman barostat. The final 200 ns MD production run was then simulated under the NPT ensemble. The long-range electrostatics were calculated with the Particle Mesh Ewald method with a cutoff of 1.0 nm on the short-range non-bonded interaction. The bond lengths were constrained with the LINCS algorithm. Trajectory analysis, root mean square deviation (RMSD), root mean square fluctuation (RMSF), radius of gyration (Rg), solvent accessible surface area (SASA), and hydrogen bonding (H-bonds) were carried out with the help of GROMACS analysis tools. The binding free energy has also been calculated with the help of the molecular mechanics Poisson–Boltzmann surface area (MM-PBSA) method [26]. For improved accuracy for 3PP0-STD and 3PP0-TOP1, the final calculations were carried out using the last 50 ns (for every 1000 frames) [27].

2.9. MTT Assay

The *T. bellirica* extract-induced cytotoxic effect on MDA-MB-231 cells was assessed with the MTT (3-(4,5-dimethylthiazol-2-yl)-2,5-diphenyltetrazolium bromide) assay. The hydroalcoholic extract dissolved in DMSO was used, with the final DMSO concentration in all the treatment wells, including the vehicle control, never to exceed 0.1% (v/v). The cells were seeded in 96-well plates and, after 24 h, treated with a range of the extract concentration (20–100 µg/mL), vehicle control (0.1% DMSO), or positive control (10 µM cisplatin) for 24 h. Following the treatment, the medium was removed and replaced with fresh medium with MTT at the final working concentration of 0.5 mg/mL. The plates were incubated for 4 h at 37°C to permit the formation of the formazan crystals. The formazan crystals were

then dissolved in the wells with the help of 100 µL DMSO per well. The absorbance measurement occurred at 570 nm with a reference at 690 nm in a microplate spectrophotometer. The experiment was undertaken in three independent biological replicates, each one with six technical replicates ($n = 3$) [24].

2.10. Statistical Analysis

Each experiment was done in three independent biological repetitions. The data were given in mean and standard deviation (SD). Values of cell viability produced during the MTT assay were transformed to the untreated control and indicated as percentage viability. The non-linear regression that employed a four-parameter logistic (4PL) model was used to estimate dose-response data to determine half-maximal inhibitory concentration (IC50) and the 95% confidence interval (CI). The one-way analysis of variance (ANOVA) was done to make statistical comparisons between groups, and then the Dunnett multiple comparisons *post hoc* test was done to evaluate the differences between the treated groups and the untreated control. $P < 0.05$ was regarded as statistically significant. All graphical analyses were done in the GraphPad Prism software [28].

3. RESULTS

3.1. Extraction Process Results

Following Soxhlet extraction, the obtained extract was concentrated using a rotary evaporator such that, upon complete evaporation, 5 g of solvent-free concentrated extract was obtained. Thereafter, the concentrated extract was subjected to LC–MS analyses. Ethanol was selected as the extraction solvent because it efficiently extracted *T. bellirica* constituents and effectively solubilized polar compounds.

3.2. LC–MS

LC–MS analysis was employed to identify phytoconstituents of *T. bellirica* seed extract. The matching was done using retention times, experimental m/z values, MS/MS fragmentation patterns, database/library matching, metabolite class, and proposed chemical structures. The mass spectra were obtained in the positive ionization mode, and the m/z values obtained were mostly between 60 and 622. Figure 1 shows the *T. bellirica* chromatogram. Table 1 enumerated the phytochemical constituents that were detected using HR-LC/MS. The 13 selected compounds were further analyzed because they were the highest chromatographic peaks and they were the big bioactive chemical groups, such as flavonoids and phenolic acids. The identification of key compounds, such as glabranin, tricin, and epigallocatechin, with distinct molecular weights and structural characteristics, demonstrated the enrichment of bioactive phytocompounds in the extract. Table 1 summarizes the identity confidence. In the absence of authentic reference standards, all identifications of compounds were tentatively identified (level of confidence 3) by accurate mass determination (mass error <5 ppm) and spectral similarity with in-house and external databases (GNPS and MassBank).

3.3. Molecular Properties and Drug-Likeness of the Phytocompounds

The pharmacological research goals were to examine the molecular properties and drug-likeness of the thirteen phytocompounds that were chosen to be included in the pharmacological research. Parameters such as molecular formula, molecular weight, HBAs, HBDs, MolLogP, MolLogS, MolPSA, MolVol, pKa, score on BBB, and number of stereocenters are calculated and presented in Table 2.

The MolSoft software was used in the generation of drug-likeness model scores of the reviewed compounds. Seven compounds were found to have positive drug-likeness scores and were chosen to undergo further pharmacological studies. The other six compounds (isoamylamine, tricin, epigallocatechin, 1,4-bis(p-tolylamino) anthraquinone, quinate, and eicosenoic acid) were eliminated because of poor drug-likeness scores, indicating poor oral bioavailability. This screening approach was based on the selection of compounds that had good physicochemical and pharmacokinetic attributes.

The evaluation of toxicological properties via the ProTox-II database and ADME characteristics through *in silico* tools yielded significant insights into the seven selected phytocompounds.

3.4. Toxicological Properties (ProTox-II Analysis)

The ProTox-II platform was used to determine the toxicology of the phytocompounds. The parameters predicted included carcinogenicity, immunotoxicity, mutagenicity, and cytotoxicity [Table 3]. Each of the seven compounds chosen had good toxicity profiles, and there was no significant evidence of carcinogenicity. Nobody anticipated significant

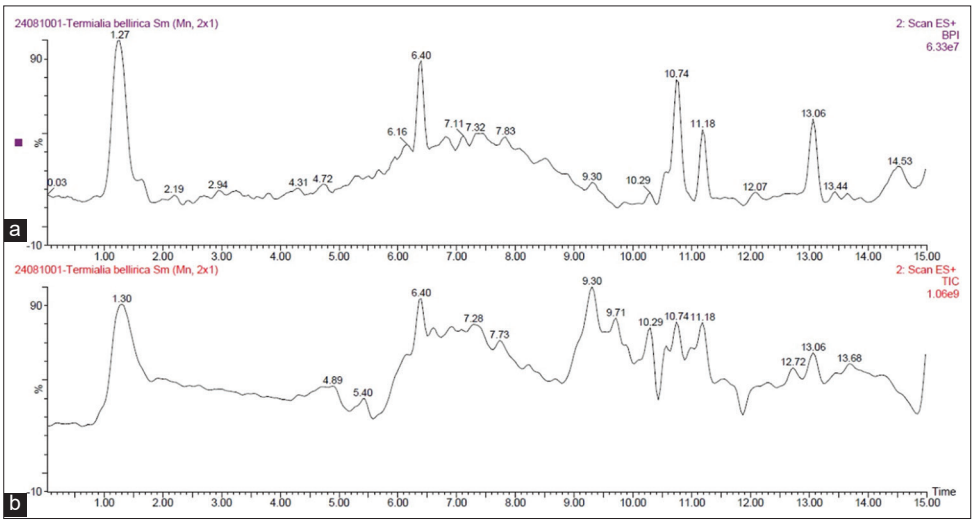

Figure 1: Chromatogram of the identified phytochemical constituents of the hydroalcoholic extract of *Terminalia bellirica* through HR–LC–MS.

Table 1: LC–MS analysis of the hydroalcoholic extract of *Terminalia bellirica.*

Compound name	RT	Structure	Molecular formula	Molecular weight (g/mol)	Adduct	Compound class
3’,5,7-Trihydroxy-4’-methoxy flavanone	1.282	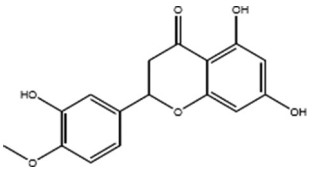	$C_{16}H_{14}O_6$	302.2788	M-H	Flavonoid
Isoamylamine	1.676	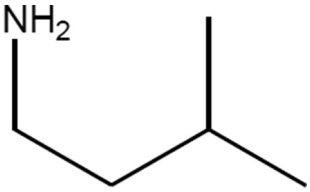	$C_5H_{13}N$	87.1634	M+H	N/A
4-Coumaroylquinic acid	1.761	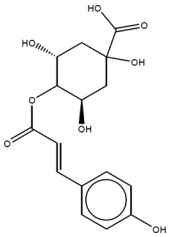	$C_{16}H_{14}O_6$	302.2788	M-H	N/A
Glabranin	6.361	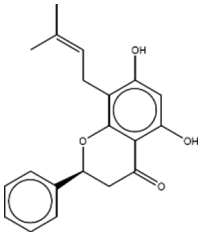	$C_{20}H_{20}O_4$	324.3704	M+H	Flavonoids
Tricin	6.601	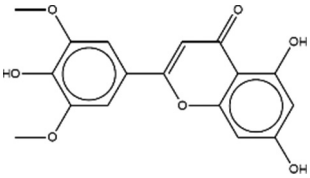	$C_{17}H_{14}O_7$	330.2889	M+H	Flavonoids
Quinate	6.652	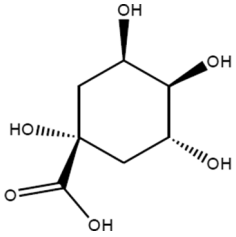	$C_7H_{12}O_6$	192.1666	M-H	N/A
Phloretin-2’-O-glucoside	7.114	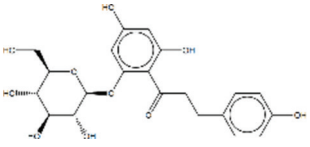	$C_{21}H_{24}O_{10}$	436.4093	M+H	N/A
6-Prenylnaringenin	7.712	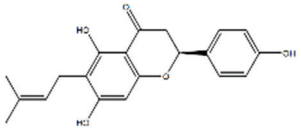	$C_{20}H_{20}O_5$	340.3698	M+H	N/A

(*Contd*...)

Table 1: (*Continued*).

Compound name	RT	Structure	Molecular formula	Molecular weight (g/mol)	Adduct	Compound class
Flavone	7.729	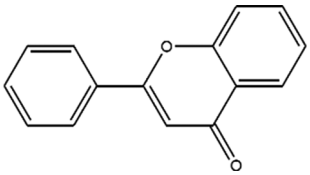	$C_{28}H_{32}O_{14}$	592.5453	M+H	Flavone C-glycosides
Epigallocatechin	7.729	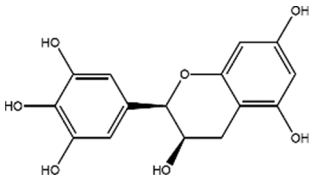	$C_{15}H_{14}O_7$	306.2675	M+H	N/A
1,4-bis (p-tolylamino) anthraquinone	9.302	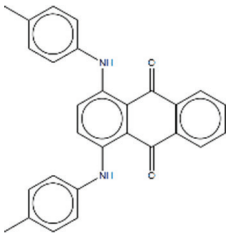	$C_{28}H_{22}N_2O_2$	418.4865	M+H	N/A
Eicosenoic acid	10.65		$C_{18}H_{34}O_2$	310.5	M+H	N/A
Fortunellin	10.739	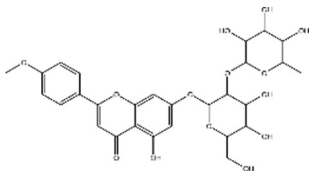	$C_{28}H_{32}O_{14}$	592.5453	M+H	Flavonoid

immunotoxic or mutagenic potentials in a couple of compounds, and cytotoxicity levels were within acceptable ranges, which justifies their use in the subsequent research.

3.5. ADME Property Analysis

The ADME properties were assessed, and it was found that the majority of the seven compounds selected had high gastrointestinal absorption and moderate/good BBB permeability. The vast majority of compounds were not associated with P-glycoprotein substrates, which means that there is a lower probability of having bioavailability limitations in the form of efflux. There was limited cytochrome P450 inhibition [Table 4], which indicates a low likelihood of drug–drug interaction. Six of them fell under the Lipinski rule of five, and Fortunellin was disqualified because of several infractions.

To integrate findings from multiple databases, six phytocompound targets were retrieved from the Swiss Target Prediction database, whereas disease-associated targets were curated through the GeneCards database. The phytocompound targets were uploaded into the STRING database to study the PPI networks shown in Figure 2 and perform KEGG pathway analysis. PPI analysis revealed significant interaction clusters, shedding light on key biological processes and molecular pathways influenced by the selected phytocompounds. KEGG pathway analysis revealed pathways potentially modulated by these targets, many of which were associated with specific disease states.

The Venn diagram juxtaposes the two datasets, “Compound Targets” (311 elements) and “Disease Targets” (18,390 elements). The analysis revealed that 281 targets (1.5%) were common to both lists, indicating potential shared biological mechanisms or interactions that could be critical for understanding therapeutic effects or drug development. The analysis also revealed that 30 targets (0.2%) are unique to the “Compound Targets” list, suggesting pathways or mechanisms that specifically appraise the compounds studied. Finally, 18,109 targets (98.3%) found only in the “Disease Targets” list indicate disease-related mechanisms not directly associated with the compounds. The large number of unique disease targets (18,109) reflects the complexity of breast cancer. However, by applying a high-confidence threshold (relevance score >10) to the GeneCards data, the analysis focused on 1,842 top-ranked targets for a more biologically relevant network. The 281 overlapping targets between this high-confidence set and the compound targets were considered the most promising for mediating the anti-breast cancer effects and were used for subsequent pathway analysis [Figure 3].

A complete network was built to describe the interactions between compound-specific targets and disease-associated targets, as shown in Figure 4 and Table 5. The network shows some key nodes and hubs to better appreciate the critical modulators in the system. The ligand–target interaction network is shown in yellow. The identified targets and their ligands were studied through molecular docking, which revealed compelling and specific interactions with important protein targets. To validate these interactions further, we performed MD simulations that revealed the stability and dynamic behavior of the docked complexes over time. These analyses confirmed worthwhile interactions and reinforced the therapeutic potential of the set of phytocompounds.

Table 2: Molecular properties and drug-likeness of the phytocompounds.

S. NO	Name of the compound	Molecular formula	Molecular weight	Number of HBA	Number of HBD	MolLogP	MolLogS	Molecular polar surface area	Molecular volume	pKa of most basic/acidic group	Blood-brain barrier score	Number of stereo centers	Drug-likeness model score
1	Isoamylamine	$C_5H_{13}N$	87.10	1	2	1.03	−0.23 (in Log (moles/L)) 51512.44 (in mg/L)	21.67 A2	103.75 A3	10.30/22.57	3.87	0	−1.37
2	Glabranin	$C_{20}H_{2O}O_4$	324.14	4	2	4.61	−4.26 (in Log (moles/L)) 17.82 (in mg/L)	52.98 A2	344.74 A3	<0./8.82	3.99	1	0.91
3	Tricin	$C_{17}H_{14}O_7$	330.07	7	3	2.53	−2.68 (in Log (moles/L)) 694.31 (in mg/L)	86.69 A2	323.54 A3	<0./6.70	2.74	0	−0.08
4	Phloretin-2'-O-glucoside	$C_{21}H_{24}O_{10}$	436.14	10	7 (>5)	0.45	−1.87 (in Log (moles/L)) 5837.71 (in mg/L)	144.94 A2	389.19 A3	<0./8.23	1.70	5	0.66
5	Flavone	$C_{18}H_{23}NO_3$	301.17	4	4	2.42	−1.61 (in Log (moles/L)) 7414.61 (in mg/L)	62.62 A2	294.71 A3	9.31/10.09	3.60	2	1.21
6	Epigallocatechin	$C_{15}H_{14}O7$	306.07	7	6 (>5)	0.26	−0.91 (in Log (moles/L)) 37829.65 (in mg/L)	105.93 A2	271.81 A3	<0./9.36	2.50	2	−0.04
7	1,4-bis (p-tolylamino) anthraquinone	$C_{28}H_{22}N_2O_2$	418.17	2	2	8.15 (>5)	−6.06 (in Log (moles/L)) 0.36 (in mg/L)	42.61 A2	414.06 A3	−2.55/21.57	3.55	0	−0.80
8	Fortunellin	$C_{28}H_{32}O_{14}$	592.18 (>500)	14 (>10)	7 (>5)	0.82	−1.79 (in Log (moles/L)) 9499.99 (in mg/L)	172.17 A2	532.32 A3	<0./9.77	1.24	10	0.70
9	3',5,7-Trihydroxy-4'-methoxy flavanone	$C_{16}H_{14}O_6$	302.08	6		2.51	−2.77 (in Log (moles/L)) 511.01 (in mg/L)	78.55 A2	283.84 A3	<0./8.29	2.89	1	0.59
10	4-Coumaroylquinic acid	$C_{16}H_{18}O_8$	338.10	8	5	−0.02	−1.34 (in Log (moles/L)) 15281.13 (in mg/L)	111.98 A2	326.25 A3	<0./4.69	2.20	2	0.03
11	Quinate	$C_7H_{12}O_6$	192.06	6	5	−2.17	−0.05 (in Log (moles/L)) 171548.56 (in mg/L)	90.69 A2	172.85 A3	<0./4.69	1.91	2	−1.06
12	6-Prenylnaringenin	$C_{20}H_{2O}O_5$	340.13	5	3	4.49	−4.44 (in Log (moles/L)) 12.24 (in mg/L)	69.85 A2	355.23 A3	<0./8.82	2.95	1	1.36
13	Eicosenoic acid	$C_{20}H_{38}O_2$	310.29	2	1	8.12 (>5)	−5.79 (in Log (moles/L)) 0.51 (in mg/L)	28.89 A2	384.40 A3	<0./4.26	4.40	0	−0.30

Table 3: Toxicological properties of the phytocompounds.

S. No	Name of compound	Carcinogenicity	Immunotoxicity	Mutagenicity	Cytotoxicity
1	Isoamylamine	No	No	No	No
2	Glabranin	No	Yes	No	No
3	Tricin	No	No	No	No
4	Phloretin-2'-O-glucoside	No	No	No	No
5	Flavone	YES	No	No	Yes
6	Epigallocatechin	No	No	No	No
7	1,4-bis (p-tolylamino) anthraquinone	Yes	No	Yes	No
8	Fortunellin	No	Yes	No	No
9	3',5,7-Trihydroxy-4'-methoxy flavanone	No	Yes	No	No
10	4-Coumaroylquinic acid	No	Yes	No	No
11	Quinate	No	No	No	No
12	6-Prenylnaringenin	No	No	No	No
13	Eicosenoic acid	No	No	No	No

Table 4: ADME properties of the phytocompounds.

S. No	Name of compound	GI absorption	Blood–brain barrier permeant	Pgp substrate	CYP1A2 inhibitor	CYP2C19 inhibitor	CYP2C9 inhibitor	CYP2D6 inhibitor	CYP3A4 inhibitor	LipinskiRule	Bioavailability score
1	Isoamylamine	High	Yes	No	No	No	No	No	No	Yes	0.55
2	Glabranin	High	Yes	No	Yes	Yes	Yes	Yes	Yes	Yes	0.55
3	Tricin	High	No	No	Yes	No	Yes	Yes	Yes	Yes	0.55
4	Phloretin-2'-O-glucoside	Low	No	Yes	No	No	No	No	No	Yes	0.55
5	Flavone	High	Yes	No	Yes	Yes	No	No	No	Yes	0.55
6	Epigallocatechin	High	No	No	No	No	No	No	No	Yes	0.55
7	1,4-bis (p-tolylamino) anthraquinone	High	No	No	Yes	Yes	No	No	No	Yes	0.55
8	Fortunellin	Low	No	Yes	No	No	No	No	Yes	No	0.17
9	3',5,7-Trihydroxy-4'- methoxy flavanone	High	No	Yes	Yes	No	No	No	Yes	Yes	0.55
10	4- Coumaroylquinic acid	Low	No	No	No	No	No	No	No	Yes	0.56
11	Quinate	Low	No	Yes	No	No	No	No	No	Yes	0.56
12	6-Prenylnaringenin	High	No	No	Yes	No	Yes	Yes	Yes	Yes	0.55
13	Eicosenoic acid	Low	No	No	Yes	No	Yes	No	No	Yes	0.85

3.6. Molecular Docking

Our docking analysis revealed that the binding affinity of protein–ligand complexes varies. The docking score was successfully used to quantify the extent of interaction between two entities, that is, ligands and proteins. Molecular docking revealed strong binding affinities for both the phytocompound 6-prenylnaringenin (3PP0-TOP1) and the standard drug doxorubicin (3PP0-STD) with the HER2 kinase domain. The calculated docking scores were −7.5 kcal/mol for 3PP0-TOP1 and −9.2 kcal/mol for 3PP0-STD. A more negative score indicates a stronger predicted binding affinity; therefore, doxorubicin showed a superior docking score compared to the phytocompound. Leu726, Ser728, Gly729, Met801, Asp845, Arg849, Asn850, Leu852, Thr862, and Asp863 are among the signature residues involved in complex interactions, indicating a stable and potentially more productive modality of binding. The comparatively high number of interacting residues in this kind of complex indicates that the ligand adopts a favorable conformation toward the protein to bind firmly, thus increasing the probability of docking. In contrast, although it is a complex of high binding affinity with a docking score of −9.2, the 3PP0-STD complex interacts with several important residues, such as LEU726, SER728, GLY729, ALA730, VAL734, ALA751, LYS753, THR798, CYS805, ASP845, ARG849, ASN850, LEU852, THR862, and ASP863. However, their interaction is comparatively stronger because it seems to have a weaker or less optimal binding orientation than its counterpart. The docking scores of the selected ligands docked to the target proteins are tabulated and provided in Table 6, along with 2D interaction images in Figure 5.

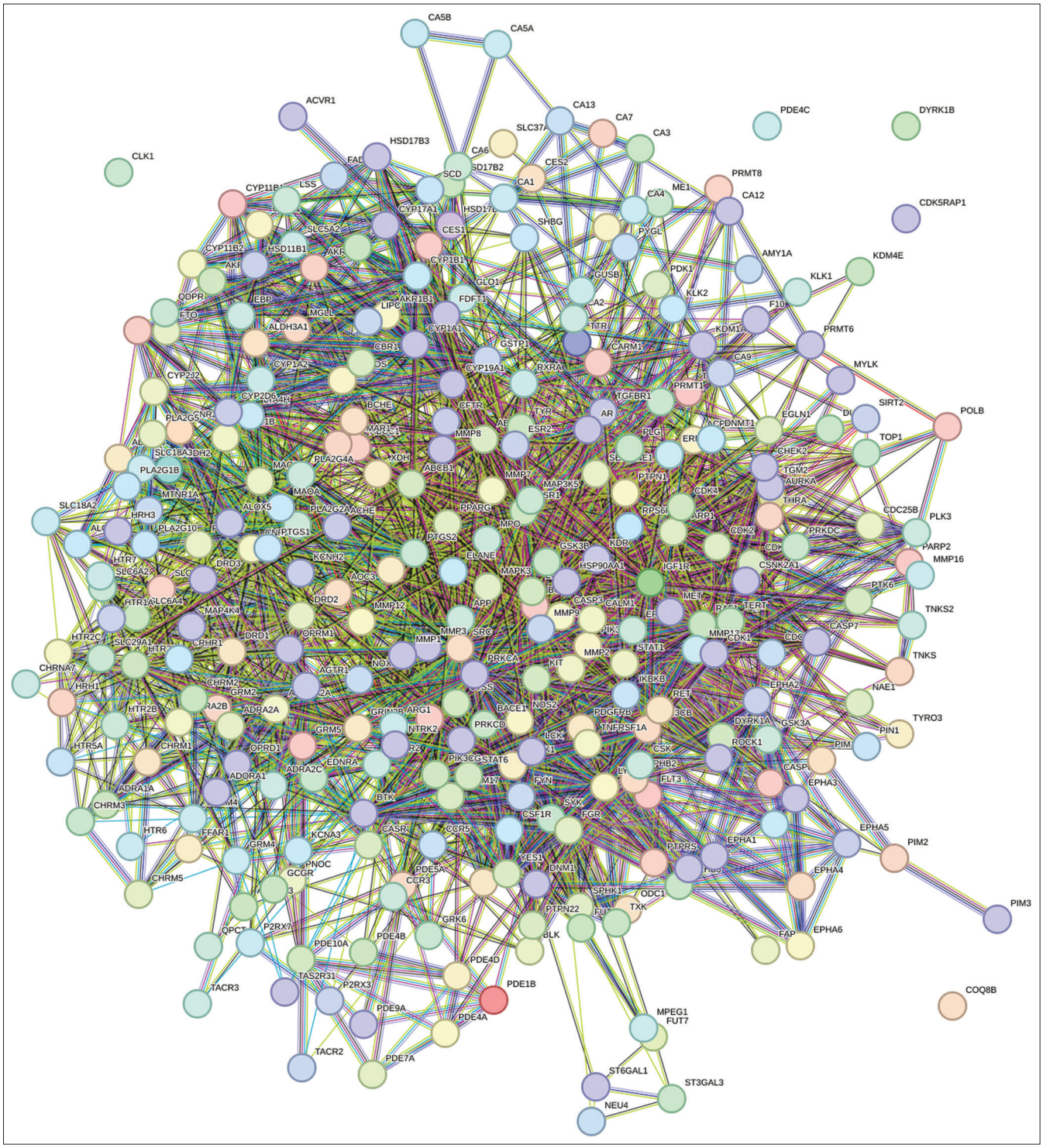

Figure 2: Probable protein–protein interaction network.

3.7. MD

All-atom MD simulation was a powerful method for studying the dynamic structural behavior of proteins and their interactions with ligands. This methodology revolutionized computer-aided drug design and research, facilitating exploration of molecular systems at atomic resolution. In the present study, MD simulations were employed to further explore conformational changes upon binding of the target protein. For the protein–ligand complex, several parameters were calculated: RMSD, RMSF, Rg, SASA, and H-bond interactions.

3.7.1. RMSD

The RMSD profiles for all systems reached a stable plateau after the initial ~50 ns, suggesting the simulations had equilibrated [Figure 6]. The average RMSD values over the production phase were 0.37 ± 0.05 nm for 3PP0-APO, 0.30 ± 0.04 nm for 3PP0-TOP1, and 0.29 ± 0.04 nm for 3PP0-STD. The lower average RMSD in the liganded

Table 5: Pathways associated with breast cancer progression modulated by phytocompounds.

Pathways	Proteins
Pathways in cancer	MAPK1, BDKRB1, MMP2, RPS6KB1, CDKN1B, FLT3, EGLN3, PDGFRA, CDK4, PDGFRB, MAPK3, PRKCG, BIRC3, PIK3CA, CDK6, CDK2, ERBB2, EGFR, CSF1R, PPARG, KIT, STAT6, MAP2K1, CXCL8, F2, TERT, CASP3, EDNRA, MET, ROCK2, MMP1, GSK3B, NOS2, HSP90AA1, GSTA1, FGFR3, PTK2, ESR2, RET, STAT1, MTOR, EGLN1, PTGS2, CASP7, GSTO1, XIAP, HSP90AB1, MMP9, ABL1, PIM1, HDAC1, AR, PIM2, PIK3CD, JAK2, ALK, BAD, MAPK8, BCL2, GSTP1, ROCK1, FGFR1, AGTR1, RAF1, ESR1, PRKCA, FGFR2, BRAF, RXRA, IKBKB, NTRK1, JAK3, TGFBR1, BDKRB2, AKT1, BIRC2, PRKCB, IGF1R, JAK1, PIK3CB
PI3K-Akt signaling pathway	MAPK1, RPS6KB1, CDKN1B, FLT3, PDGFRA, CDK4, PDGFRB, MAPK3, KDR, PIK3CA, CDK6, CDK2, ERBB2, EGFR, NTRK2, FLT1, CSF1R, KIT, NOS3, MAP2K1, INSR, CHRM1, MET, GSK3B, HSP90AA1, FGFR3, PTK2, PDPK1, EPHA2, MTOR, MCL1, HSP90AB1, SYK, PIK3CD, JAK2, BAD, BCL2, FGFR1, CHRM2, RAF1, PRKCA, FGFR2, PIK3CG, RXRA, IKBKB, NTRK1, JAK3, AKT1, ITGB3, IGF1R, JAK1, PIK3CB
MAPK signaling pathway	TNFRSF1A, MAPK1, DUSP3, MAPK14, FLT3, CDC25B, PDGFRA, PDGFRB, MAPK3, MAP3K8, PRKCG, KDR, ERBB2, EGFR, NTRK2, FLT1, CSF1R, KIT, DUSP16, MAP2K1, INSR, CASP3, MET, FGFR3, EPHA2, MAP3K5, CACNA1S, MAPKAPK2, PLA2G4A, MAPK8, FGFR1, RAF1, PRKCA, FGFR2, BRAF, STK3, IKBKB, NTRK1, TGFBR1, AKT1, IRAK4, PRKCB, IGF1R
HIF-1 signaling pathway	MAPK1, SERPINE1, RPS6KB1, CDKN1B, EGLN3, MAPK3, PRKCG, PIK3CA, ERBB2, EGFR, FLT1, NOS3, MAP2K1, INSR, NOS2, MTOR, EGLN1, PIK3CD, PDK1, BCL2, PRKCA, AKT1, PRKCB, IGF1R, PIK3CB
ErbB signaling pathway	MAPK1, RPS6KB1, CDKN1B, MAPK3, PRKCG, PIK3CA, ERBB2, EGFR, MAP2K1, GSK3B, PTK2, MTOR, ABL1, SRC, PIK3CD, BAD, MAPK8, RAF1, PRKCA, BRAF, AKT1, PRKCB, PIK3CB
Estrogen signaling pathway	MAPK1, MMP2, MAPK3, PIK3CA, EGFR, NOS3, MAP2K1, PRKCD, HSP90AA1, ESR2, HSP90AB1, MMP9, SRC, PIK3CD, BCL2, OPRM1, RAF1, ESR1, AKT1, PIK3CB
mTOR signaling pathway	TNFRSF1A, MAPK1, RPS6KB1, MAPK3, PRKCG, PIK3CA, MAP2K1, INSR, GSK3B, PDPK1, MTOR, PIK3CD, RAF1, PRKCA, BRAF, IKBKB, AKT1, PRKCB, IGF1R, PIK3CB
p53 signaling pathway	SERPINE1, CDK4, CDK6, CDK2, CASP3, CDK1, BCL2, CHEK1

Table 6: Docking scores and interactions with proteins.

Protein–Ligand Complex	Docking score	Interactions
3PP0-Top1 (155094) 6-Prenylnaringenin	−7.5	LEU726, SER728, GLY729, MET801, ASP845, ARG849, ASN850, LEU852, THR862, ASP863
3PP0-standard (31703) doxorubicin	−9.2	LEU726, SER728, GLY729, ALA730, VAL734, ALA751, LYS753, THR798, CYS805, ASP845, ARG849, ASN850, LEU852, THR862, ASP863

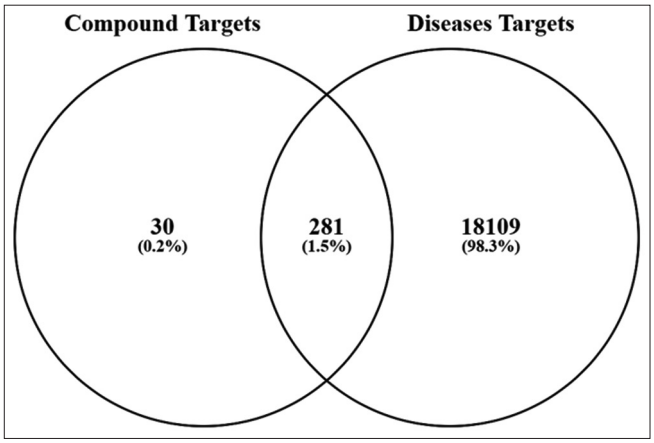

Figure 3: Venn diagram of compound targets and disease targets.

systems suggested a potential stabilizing effect upon ligand binding. It was important to note that these observations are based on single simulation runs; future studies incorporating multiple independent replicates and statistical testing would be required to confirm the significance of these differences.

3.7.2. RMSF

RMSFs were used to track the movements of individual residues and flexible sections of a protein over MD runs. Thus, with the help of RMSF calculations during simulations, we measured how ligand binding affects a protein. Typically, minor regular protein conformations, such as sheets and helices, exhibited lower RMSF, whereas loosely ordered loop regions presented higher RMSF values. The RMSD values for all the peaks were computed and plotted per residue for the 3PP0-APO, 3PP0-TOP1, and 3PP0-STD complexes [Figure 7]. The average RMSF values of 3PP0-APO, 3PP0-TOP1, and 3PP0-STD were 0.18 ± 0.11 nm, 0.17 ± 0.10 nm, and 0.17 ± 0.09 nm, respectively. The RMSF distributions of these three complexes, including the ligand, remained largely unchanged compared with those of the STD and APO complexes.

3.7.3. Rg

To measure the dynamic stability and solidity of the 3PP0-APO, 3PP0-TOP1, and 3PP0-STD complexes, the Rg values were calculated and graphed over time [Figure 8]. The average Rg values for 3PP0-APO, 3PP0-TOP1, and 3PP0-STD were 2.00 ± 0.02 nm, 2.01 ± 0.02 nm, and 2.01 ± 0.02 nm, respectively. Compared with the 3PP0-STD complex system, the 3PP0-TOP1 complex system presented similar Rg values, indicating that both complex systems had comparable compactness.

3.7.4. SASA

The SASA was a useful parameter for evaluating the accessibility of a protein molecule in a solvent environment. In this study, to determine the impact of 3PP0-STD binding on the solvent accessibility of the target, the SASA values were calculated and plotted [Figure 9]. The plot revealed a comparable pattern in the SASA values of 3PP0-APO, 3PP0-TOP1, and 3PP0-STD. The average SASA values for 3PP0-APO, 3PP0-TOP1, and 3PP0-STD were determined to be 150.41 ± 4.24 nm, 156.27 ± 3.27 nm, and 157.40 ± 3.52 nm, respectively. The SASA values showed fair equilibration without significant fluctuations throughout the simulation.

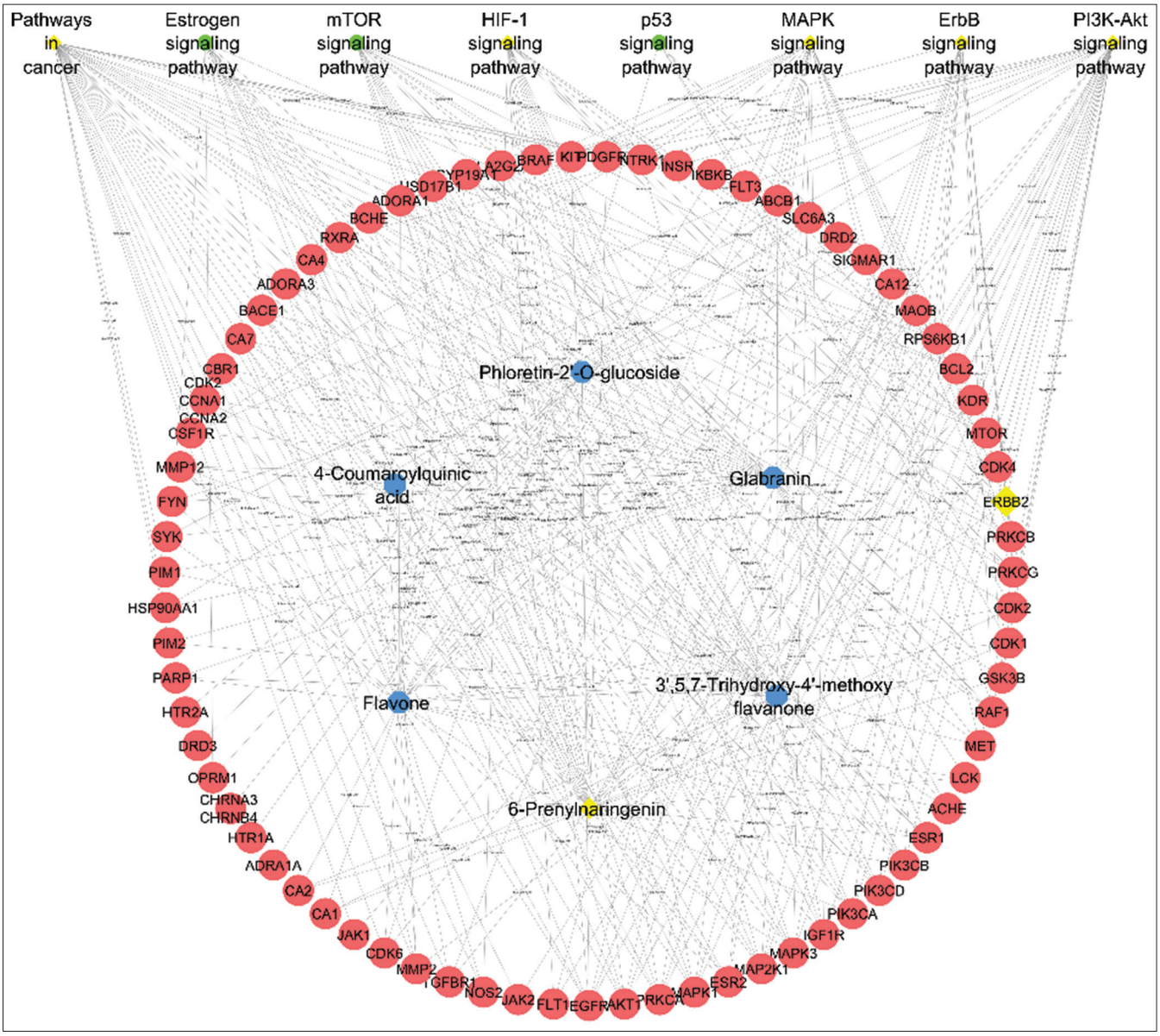

Figure 4: Network representation of compounds, proteins, and pathway interactions.

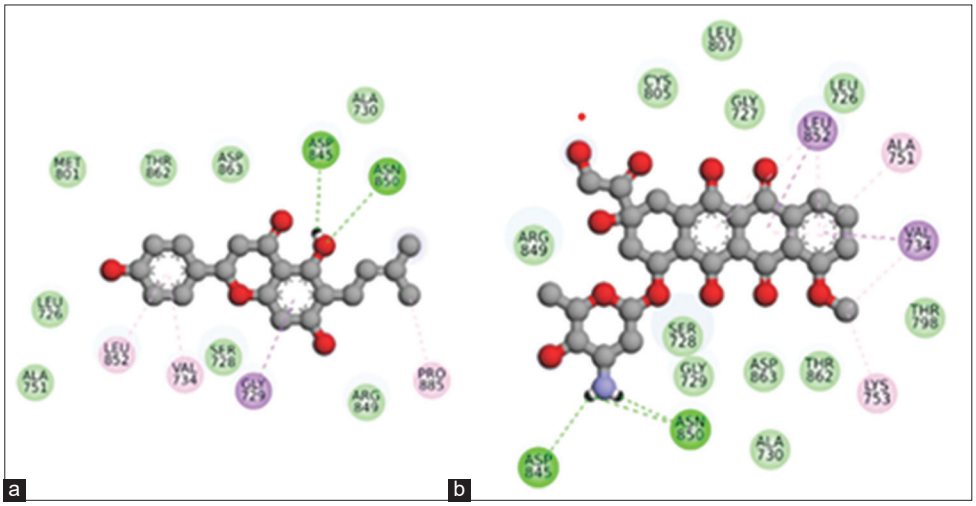

Figure 5: 2D images of the protein–ligand interactions of (a) 3PP0-TOP 1 (6-Prenylnaringenin) and (b) 3PP0-STD complexes.

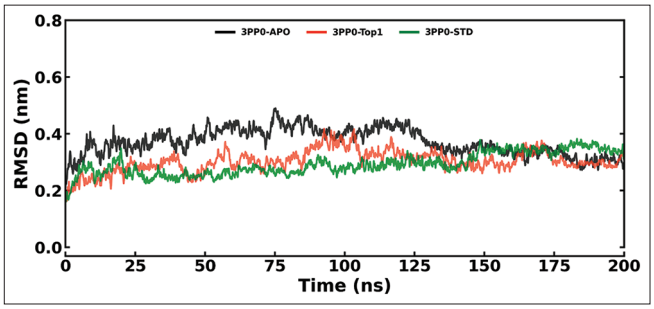

Figure 6: Root mean square deviation conformational dynamics analysis of 3PP0-APO, 3PP0-TOP1, and 3PP0-STD

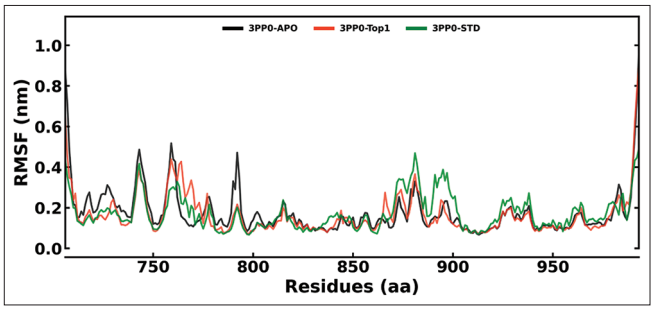

Figure 7: Root mean square fluctuation conformational dynamics analysis of the 3PP0-APO, 3PP0-TOP1, and 3PP0-STD complexes.

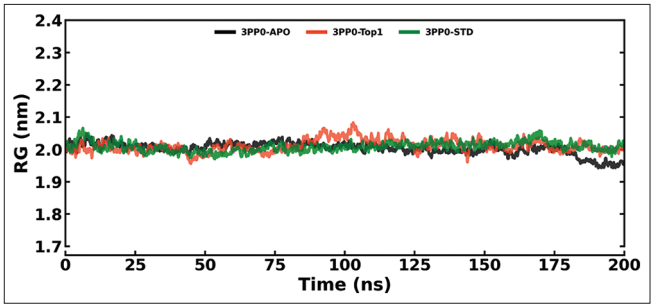

Figure 8: Radius of gyration conformational dynamics analysis of the 3PP0-APO, 3PP0-TOP1, and 3PP0-STD complexes.

3.7.5. Intra- and Inter-hydrogen Bonds

To examine the stability of protein interactions (3PP0-APO, 3PP0-TOP1, and the 3PP0-STD complex), the formation of intra- and inter-hydrogen bonds played a vital role. We examined the time-dependent behavior of the intrahydrogen bonds of the 3PP0-APO, 3PP0-TOP1, and 3PP0-STD complexes and plotted the results [Figure 10]. The average intra-H-bond values for 3PP0-APO, 3PP0-TOP1, and the 3PP0-STD complex were determined to be 205.65 ± 8.09 nm, 201.65 ± 8.07 nm, and 202.42 ± 7.43 nm, respectively. The plot revealed that, despite more hydrogen bonds being formed in the 3PP0-TOP1 and 3PP0-STD complexes than in the 3PP0-APO form of the protein, the results indicated that the 3PP0-TOP1 and 3PP0-STD complexes were more stable than the 3PP0-APO form.

The formation of hydrogen bonds played a crucial role in assessing the stability of protein–ligand interactions. In this study, we investigated the time-dependent behavior of hydrogen bonds between 3PP0-APO, 3PP0-TOP1, and 3PP0-STD and plotted the results [Figure 11]. Our analysis indicated that the docked complex remained stable during the simulation, maintained by at least 1–6 hydrogen bonds with 3PP0-TOP1 and 1–4 hydrogen bonds with the 3PP0-STD complex.

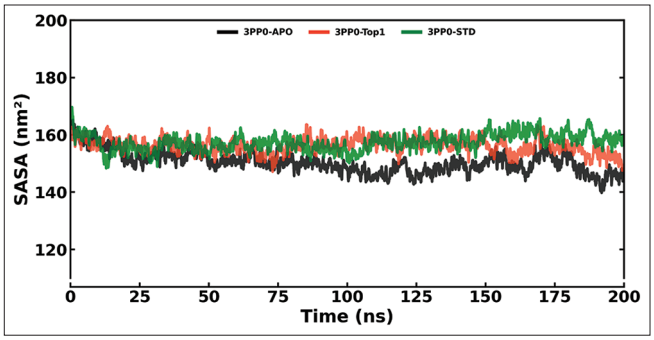

Figure 9: Solvent accessible surface area conformational dynamics analysis of the 3PP0-APO, 3PP0-TOP1, and 3PP0-STD complexes.

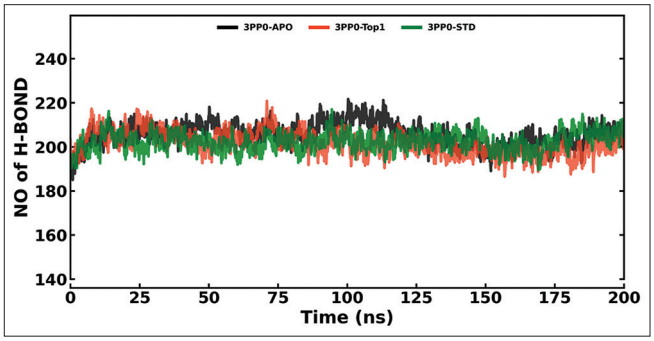

Figure 10: Intramolecular hydrogen bonds of 3PP0-APO, 3PP0-TOP1, and 3PP0-STD during the simulation time.

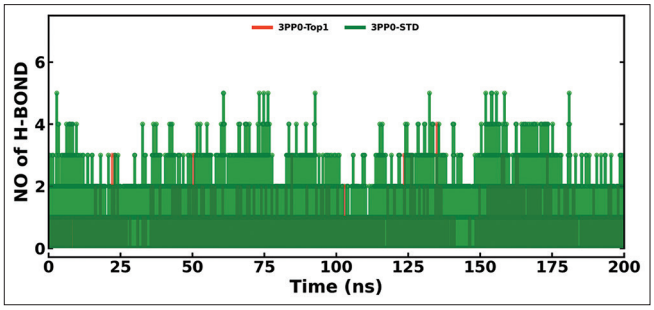

Figure 11: Intermolecular hydrogen bonds between proteins and ligands during the simulation.

The MD analyses and conclusions presented herein are based on single 200 ns simulations for each system. While the trajectories appear stable and converged based on the RMSD and other parameters, we note that these findings represent a preliminary investigation. More robust conclusions regarding convergence and statistical significance would require multiple independent simulation replicates, which is a recognized direction for future work

3.8. Principal Component Analysis (PCA)

To explore the collective movements in 3PP0-APO, 3PP0-TOP1, and 3PP0-STD, we conducted PCA. The initial few eigenvectors (EVs) played a crucial role in the global motion of a protein molecule. We carried out PCA using GROMACS to study the conformational dynamics of 3PP0-APO, 3PP0-TOP1, and 3PP0-STD during the

simulation [Figure 12]. The time evolution of PCA suggested that the overall flexibility of the 3PP0-APO, 3PP0-TOP1, and 3PP0-STD complexes was reduced on both EVs, implying stability. The plot clearly showed that the 3PP0-APO, 3PP0-TOP1, and 3PP0-STD complexes occupied almost all the conformational motions. In general, the lower amount of movement observed in 3PP0-TOP1 and 3PP0-STD suggests that 3PP0-TOP1 and 3PP0-STD did not significantly affect the target conformation and dynamics, thus supporting the stability of the complex.

3.9. Free Energy Landscapes (FELs)

In general, FEL analysis was considered a powerful methodology that has been used to map the protein folding landscape, including protein stability. FEL plots (FEL plots) provided insight into the conformations sampled by a protein structure. Here, we generated FEL plots on PC1 and PC2 [Figure 13], where the blues you see deeper into the bowl indicate a more stable (lower energy) protein conformation. The 0–14 kJ/mol and 0–16 kJ/mol energy ranges were recorded in the 3PP0-APO (A) and 3PP0-TOP1 and 3PP0-STD simulations (B). According to their FEL plots, the 3PP0-TOP1 and 3PP0-STD complexes exhibit a single global minimum inside a basin that is large compared with the local maxima. The results showed that 3PP0-TOP1 and 3PP0-STD do not induce any significant conformational differences in the target structure and thus stabilize it.

3.10. MM-PBSA

To determine the binding affinity of 3PP0-TOP1 and 3PP0-STD, we examined the relative binding strength of the summed protein energy. Table 7 compares the binding strengths of 3PP0-TOP1 and 3PP0-STD with respect to the inhibitors computed via the MM-PBSA method. Across a stable simulation trajectory, we calculated residue-level contributions to the interaction energy.

Binding free energy calculations were performed using the MM-PBSA method implemented in g_mmpbsa. Values represent mean ± SD calculated from 1000 frames extracted at 50 ps intervals from the last 50 ns of the production MD trajectory. Entropic contributions were not included in the calculations. The large positive polar solvation energies are consistent with the desolvation penalty typically observed for charged/polar groups upon binding

3.11. MTT Assay

The MTT assay was used to prove *in vitro* anticancer effects of the *T. bellirica* seed extract on MDA-MB-231 cells. A 24 h exposure to the extract had an effect of reducing cell viability in a concentration-dependent manner. The vehicle control (0.1% DMSO) has not shown significant cytotoxicity; cell viability of the vehicle control was 98.5% 1.2% as compared to that of the untreated control, further confirming that the vehicle control observed was due to the extract and not the solvent. The positive control, cisplatin (10 µM), resulted in a significant cause of the cell viability of 9.3 ± 0.7%. Non-linear regression analysis of the non-linear regression gave a determination of the IC50 value of the extract to be 57.83 ug/mL (95% confidence interval: 55.12–60.67 ug/mL). These data were given in terms of the mean SD of three independent biological replicates. One-way ANOVA and *post hoc* Dunnett test were used to compare the statistical significance, and all extract concentrations were significantly different than the control ($P < 0.001$). The findings are shown in Figures 14 and 15.

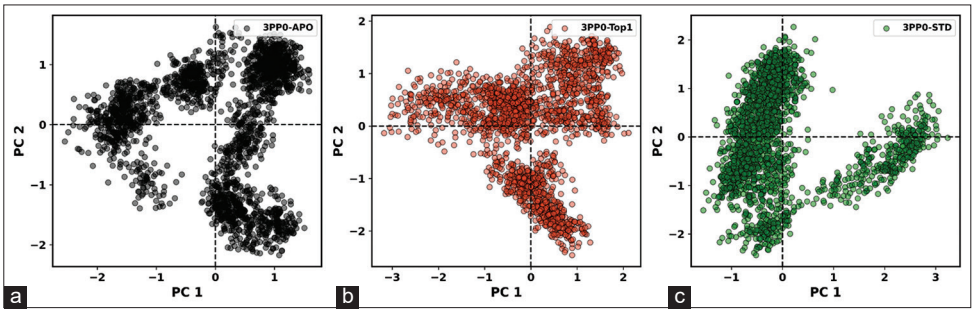

Figure 12: (a-b)Principal component analysis 2D projection plot showing the conformation sampling of 3PP0-APO, 3PP0-TOP1, and 3PP0-STD on PC1 and PC2.

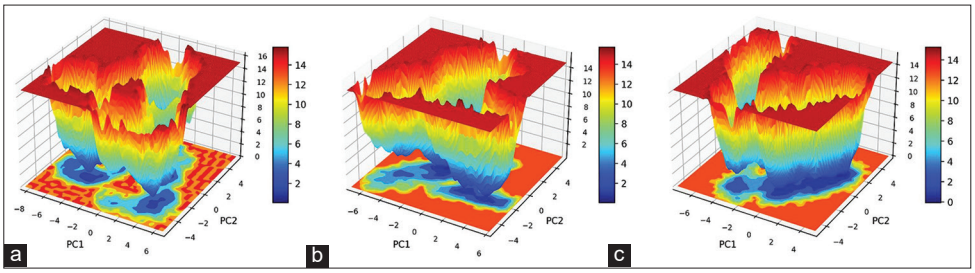

Figure 13: Free energy landscape plots for the (a) 3PP0-APO, (b) 3PP0-TOP1, and (c) 3PP0-STD complexes.

Table 7: MM-PBSA binding free energy components for the 3PP0-TOP1 and 3PP0-STD complexes. Values are mean±standard deviation (kJ/mol) calculated from 1000 frames.

System	van der Waals energy (kJ/mol)	Electrostatic energy (kJ/mol)	Polar solvation energy (kJ/mol)	Binding energy (kJ/mol)
3PP0-TOP1	−248.10±14.24	−21.67±13.34	132.25±27.80	−162.33±11.60
3PP0-STD	−221.18±11.89	−51.22±22.29	171.80±35.94	−123.41±13.29

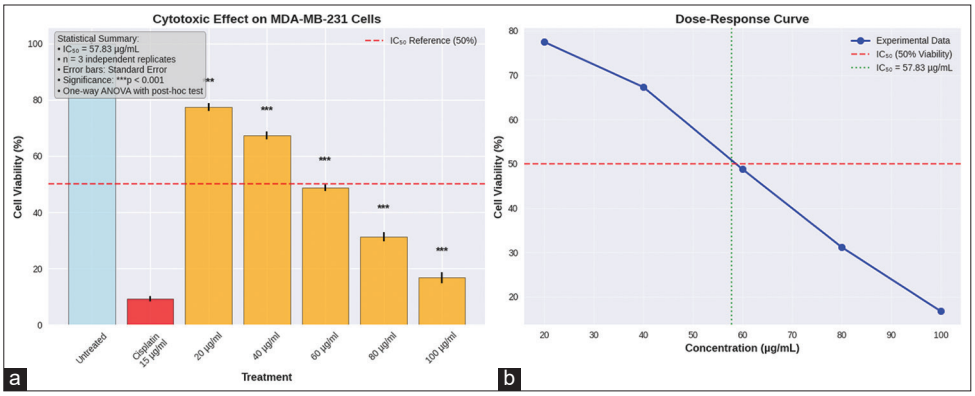

Figure 14: Cytotoxic effect of *Terminalia bellirica* extract on MDA-MB-231 cells determined by MTT assay. (a) Bar graph representing percentage cell viability at different concentrations (10–100 µg/mL) of *T. bellirica* extract after 24-h treatment, showing a dose-dependent reduction in viability compared to the untreated control. (b) Non-linear regression dose–response curve of *T. bellirica* extract illustrating the half-maximal inhibitory concentration value (57.83 µg/mL; 95% confidence interval: 51.12–60.67 µg/mL). Data are presented as mean ± standard deviation (n = 3).

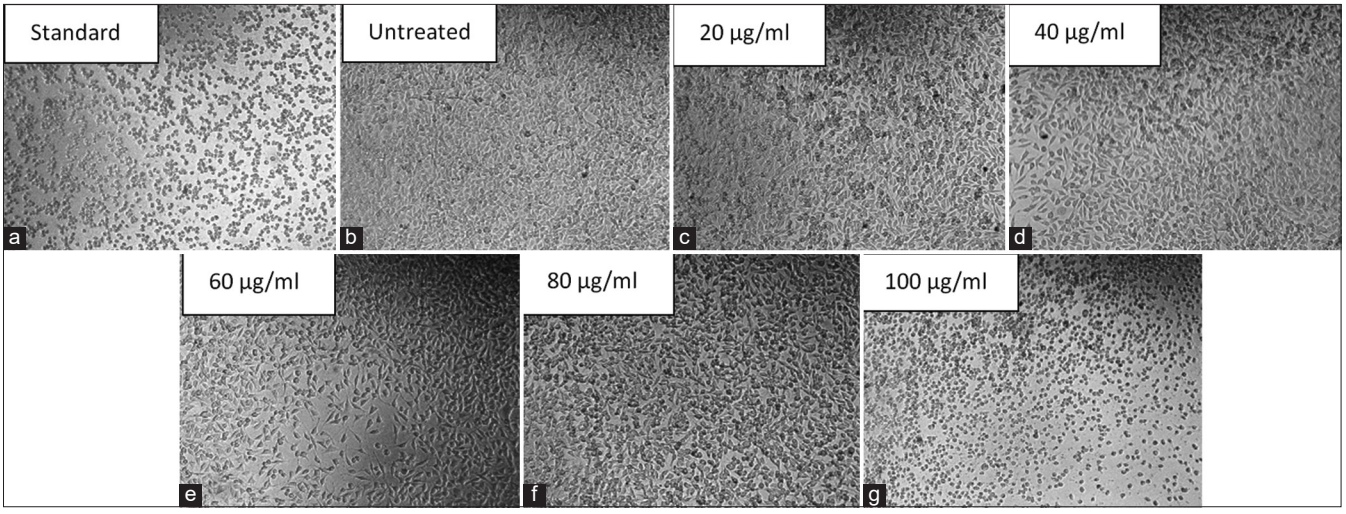

Figure 15: Morphological effects of the standard and extract on the MDA-MB-231 cell line. Representative bright-field micrographs (10× magnification) showing MDA-MB-231 cells after 24-h treatment with (a) untreated control, (b) vehicle control (0.1% DMSO), (c) 20 µg/mL, (d) 40 µg/mL, (e) 60 µg/mL, (f) 80 µg/mL, (g) 100 µg/mL of *Terminalia bellirica* extract, and (h) 10 µM cisplatin (positive control).

4. DISCUSSION

This study underscores the therapeutic potential of *T. bellirica*, especially in breast cancer conditions, and provides a strong basis for integrating native knowledge systems with current drug discovery methods. A thorough phytochemical analysis through LC–MS established diverse chemical profiles that confirmed the richness of bioactive compounds in the plant [26]. Among the 13 identified compounds, some strongly implicated by previous mechanistic data are antioxidants that modulate cell signaling pathways and induce apoptosis in cancer cells [29]. These compounds are specifically involved in mechanisms critical for suppressing breast cancer, such as the inhibition of estrogen receptor signaling, the reduction in angiogenesis, and the modulation of inflammatory pathways [30]. These strong bioactivity profiles confirmed the traditional use of *T. bellirica* in herbal medicines, particularly those related to inflammation and cancer-related treatments, especially those focused on hormone-related malignancies such as breast cancer. *In silico* studies have provided strong evidence of the drug-like and pharmacokinetic viability of these compounds, especially in terms of breast cancer treatment [31]. ADME profiling and toxicity predictions underscore the fit for a surgical application with limited chances for off-target effects or adverse reactions. The pharmacokinetic advantages noted with the extracts of *T. bellirica* also make them reliable candidates for future research into their use in breast cancer therapy because of the existing challenges of systemic toxicity or the oncological development of resistance against hormonal and targeted therapies. Importantly, these compounds exhibit high gastrointestinal absorption and low hepatotoxicity, which are key features of oral chemotherapy [32]. The ability of these compounds to pierce the BBB opens avenues for the spread of metastatic breast cancer to the brain, hence widening the therapeutic spectrum of these compounds. Network pharmacology and molecular docking studies further elucidated the multitarget mechanisms underlying the anticancer potential of *T. bellirica* phytocompounds in the context of breast cancer. Important targets, such as ERBB2, Akt1, MAPK1, EGFR, VEGFA, and ESR1 (estrogen receptor alpha), were identified, suggesting that these compounds could significantly affect pathways critical for the progression of this disease. Interestingly, pathways known to regulate cell growth, survival, and proliferation in breast cancer, such as the PI3K-Akt and MAPK signaling pathways, were also highly enriched. In addition, targeting the HIF-1 signaling pathway,

which is highly associated with tumor hypoxia and angiogenesis, also hints at possible antiangiogenic effects that might inhibit tumor growth and metastasis [33].

The ability of these compounds to modulate estrogen receptor signaling pathways enhances their pertinence in hormone receptor-positive breast cancer. Molecular docking and dynamics simulations confirmed that these phytocompounds are stable and specific in their interactions with their targets [34,35]. High binding affinities during extensive periods of simulation prove their value as potential inhibitors/modulators in breast cancer treatment. This is a typical multi-pathway approach inherent in breast cancer pathophysiology and emphasizes a striking advantage in polypharmacology with plant-based agents. The extracts of *T. bellirica* displayed significantly greater anticancer activity against MDA-MB-231 breast cancer cells, with an IC50 of 57.83 µg/mL, demonstrating potent cytotoxicity. These *in silico* conclusions were convincingly corroborated by the results of the MTT assay, which revealed that the extract significantly reduced cell viability. The decrease in cell viability in a dose-dependent manner may be due to the presence of bioactive compounds with antiproliferative activities [36]. The extract of *T. bellirica* showed notable cytotoxicity to MDA-MB-231 cells with IC50 = 57.83 µg/mL. Even though the presentation of a direct, statistically adequate comparative study with cisplatin could not be within the scope of this study, the activity observed here suggests that the extract of *T. bellirica* is deserving of exploration as a source of anticancer compounds. The *in silico* predictions define a hypothetical mechanism for this activity that suggests possible interaction with significant cancer-related targets and pathways. Such computational conclusions must be experimentally confirmed with isolation of actives, thorough mechanistic assays (e.g., apoptosis, cell cycle studies), as well as direct comparative studies with conventional chemotherapeutic agents. Venturelli *et al*. reported that 6- and 8-prenylnaringenin (PN) were involved in the inhibition of cellular histone deacetylases, which were responsible for human melanoma disease [37]. The results validated in triplicate will direct further studies to explore its mechanism and *in vivo* efficacy. Overall, these findings provide hope for the development of *T. bellirica* as a candidate for cancer therapy.

This study has some limitations. The compound identifications with the LC-MS are preliminary и must be confirmed with authentic standards. The strategy of network pharmacology, though robust, relies on computational predictions; the biological relevance of the identified targets и pathways must be confirmed experimentally. The *in silico* ADME и toxicity profiles are predictive и must be confirmed with *in vitro* и *in vivo* studies. The future studies will be guided toward the isolation of the most relevant bioactive compounds, the confirmation of their mechanisms of action with biological assays, и the confirmation of the pharmacokinetic safety profiles.

5. CONCLUSION

This research highlights the use of natural products such as *T. bellirica* in breast cancer drug discovery. Scientific evidence such as this will easily pave the way for further exploratory and clinical research on other phytocompounds from *T. bellirica* with the aim of developing novel plant-originating chemotherapeutics for breast cancer therapy. Therefore, future studies must aim to establish *in vitro* and *in vivo* validations of these findings, optimize extraction methods for maximum yield and purity, and investigate the synergistic effects of these compounds in combination with conventional breast cancer treatments such as hormonal agents and targeted inhibitors. Such a holistic approach would undoubtedly bode well for the future development of safer, more effective treatment modalities for breast cancer, particularly in overcoming drug resistance and minimizing toxicity.

6. AUTHOR CONTRIBUTIONS

All authors made substantial contributions to conception and design, acquisition of data, or analysis and interpretation of data; took part in drafting the article or revising it critically for important intellectual content; agreed to submit to the current journal; gave final approval of the version to be published; and agree to be accountable for all aspects of the work. All the authors are eligible to be author as per the International Committee of Medical Journal Editors (ICMJE) requirements/guidelines.

7. FUNDING

There is no funding to report.

8. CONFLICTS OF INTEREST

The authors report no financial or any other conflicts of interest in this work.

9. ETHICAL APPROVALS

This study does not involve experiments on animals or human subjects.

10. DATA AVAILABILITY

All the data is available with the authors and shall be provided upon request.

11. PUBLISHER'S NOTE

All claims expressed in this article are solely those of the authors and do not necessarily represent those of the publisher, the editors and the reviewers. This journal remains neutral with regard to jurisdictional claims in published institutional affiliation.

12. USE OF ARTIFICIAL INTELLIGENCE (AI)-ASSISTED TECHNOLOGY

The authors declare that they have not used artificial intelligence (AI)-tools for writing and editing of the manuscript, and no images were manipulated using AI.

REFERENCES

1. Cock IE. The medicinal properties and phytochemistry of plants of the genus *Terminalia* (Combretaceae). Inflammopharmacology. 2015;23:203-29. https://doi.org/10.1007/s10787-015-0246-z
2. Hossain MA, Uddin MS, Shumi W, Shukor NA. Depulping of fruits and soaking the seeds enhances the seed germination and initial growth performance of *Terminalia belerica* Roxb. Seedlings. Am J Plant Sci. 2014;5(5):714-25. https://doi.org/10.4236/ajps.2014.55086
3. Kuniyal CP, Purohit V, Butola JS, Sundriyal RC. Seed size correlates seedling emergence in *Terminalia bellirica*. South Afr J Bot. 2013;87:92-4. https://doi.org/10.1016/j.sajb.2013.03.016
4. Hegde SN, Lavanya Devi K, Choudhary M, Menon N, Singh G. A comprehensive metabolome profiling of *Terminalia chebula*, *Terminalia bellirica*, and *Phyllanthus emblica* to explore the medicinal potential of triphala. Sci Rep. 2024;14:31635. https://doi.org/10.1038/s41598-024-80544-6

5. Chalise JP, Acharya K, Gurung N, Bhusal RP, Gurung R, Skalko-Basnet N, *et al*. Antioxidant activity and polyphenol content in edible wild fruits from Nepal. Int J Food Sci Nutr. 2010;61(4):425-32. https://doi.org/10.3109/09637481003591590
6. Dharmaratne MP, Manoraj A, Thevanesam V, Ekanayake A, Kumar NS, Liyanapathirana V, *et al*. *Terminalia bellirica* fruit extracts: *In-vitro* antibacterial activity against selected multidrug-resistant bacteria, radical scavenging activity and cytotoxicity study on BHK-21 Cells. BMC Complement Altern Med. 2018;18(1):325. https://doi.org/10.1186/s12906-018-2382-7
7. Chang Z, Jian P, Zhang Q, Liang W, Zhou K, Hu Q, *et al*. Tannins in *Terminalia bellirica* inhibit hepatocellular carcinoma growth by regulating EGFR-signaling and tumor immunity. Food Funct. 2021;12(8):3720-39. https://doi.org/10.1039/d1fo00203a
8. Pinmai K, Chunlaratthanabhorn S, Ngamkitidechakul C, Soonthornchareon N, Hahnvajanawong C. Synergistic growth inhibitory effects of *Phyllanthus emblica* and *Terminalia bellirica* extracts with conventional cytotoxic agents: Doxorubicin and cisplatin against human hepatocellular carcinoma and lung cancer cells. World J Gastroenterol. 2008;14(10):1491-7. https://doi.org/10.3748/wjg.14.1491
9. Bakchi B, Krishna AD, Sreecharan E, Ganesh VB, Niharika M, Maharshi S, *et al*. An overview on applications of SwissADME web tool in the design and development of anticancer, antitubercular and antimicrobial agents: A medicinal chemist's perspective. J Mol Struct. 2022;1259:132712. https://doi.org/10.1016/j.molstruc.2022.132712
10. Ononamadu CJ, Seidel V. Exploring the antidiabetic potential of *Salvia officinalis* using network pharmacology, molecular docking and ADME/drug-likeness predictions. Plants (Basel). 2024;13:2892. https://doi.org/10.3390/plants13202892
11. El Rhabori S, Alaqarbeh M, El Allouche Y, Naanaai L, El Aissouq A, Bouachrine M, *et al*. Exploring innovative strategies for identifying anti-breast cancer compounds by integrating 2D/3D-QSAR, molecular docking analyses, ADMET predictions, molecular dynamics simulations, and MM-PBSA approaches. J Mol Struct. 2025;1320:139500. https://doi.org/10.1016/j.molstruc.2024.139500
12. Gupta R, Singh RL, Dwivedi N. *In vitro* antioxidant activity and gc-ms analysis of the ethanolic extracts of *Terminalia bellirica* roxb (baheda). Int J Pharm Pharm Sci. 2016;8:275-82. https://doi.org/10.22159/ijpps.2016v8i11.14175
13. Sobeh M, Mahmoud MF, Hasan RA, Abdelfattah MA, Osman S, Rashid HO, *et al*. Chemical composition, antioxidant and hepatoprotective activities of methanol extracts from leaves of *Terminalia bellirica* and *Terminalia sericea* (Combretaceae). PeerJ. 2019;7:e6322. https://doi.org/10.7717/peerj.6322
14. Ke Z, Wang G, Yang L, Qiu H, Wu H, Du M, *et al*. Crude terpene glycoside component from radix paeoniae rubra protects against isoproterenol-induced myocardial ischemic injury via activation of the PI3K/AKT/MTOR signaling pathway. J Ethnopharmacol. 2017;206:160-9. https://doi.org/10.1016/j.jep.2017.05.028
15. Vago R, Bettiga A, Salonia A, Ciuffreda P, Ottria R. Development of new inhibitors for N-acylethanolamine-hydrolyzing acid amidase as promising tool against bladder cancer. Bioorg Med Chem. 2017;25:1242-9. https://doi.org/10.1016/j.bmc.2016.12.042
16. Elizabeth LA, Bupesh G, Susshmitha R. *In vitro* antioxidant efficacy of *Terminalia bellirica* seed extract against free radicals. Int J Pharm Sci Res. 2017;8:4659-65. https://doi.org/10.13040/ijpsr.0975-8232.8(11).4659-65
17. Patil SB, Kuvalekar MB, Yaraguppi DA, Prasanth DS, Halkavatagi SG, Tennalli GB, *et al*. Exploring the efficacy of *Benincasa hispida* extract on obesity linked inflammatory bowel disease by integrating computational analysis and experimental validations. Sci Rep. 2025;15(1):14426. https://doi.org/10.1038/s41598-025-99256-6
18. Channalli SR, Pattanashetti L, Patil SB, Yaraguppi DA, Prasanth DS, Halkavatagi SG, *et al*. Deciphering the multitarget neuroprotective potential of *Ficus microcarpa* L. f. Leaf extract: Insights from phytochemical, computational, and experimental approaches. Chem Biodivers. 2025;23:e02568. https://doi.org/10.1002/cbdv.202502568
19. Banerjee P, Kemmler E, Dunkel M, Preissner R. ProTox 3.0: A webserver for the prediction of toxicity of chemicals. Nucleic Acids Res. 2024;52(W1):W513-20. https://doi.org/10.1093/nar/gkae303
20. Mane RR, Yaraguppi DA, Bagewadi ZK, Kamanna K. Organocatalysed synthesis of N-(4-oxo-2-phenyl-1,2-dihydroquinazolin-3(4 h)-yl) isonicotinamide: Computational, electrochemical, drug-likeness and antimicrobial studies. 3 Biotech. 2025;15(1):30. https://doi.org/10.1007/s13205-024-04188-z
21. Yan L, Zhang Z, Liu Y, Ren S, Zhu Z, Wei L, *et al*. Anticancer activity of erianin: Cancer-specific target prediction based on network pharmacology. Front Mol Biosci. 2022;9:862932. https://doi.org/10.3389/fmolb.2022.862932
22. Huang F, Fu M, Li J, Chen L, Feng K, Huang T, *et al*. Analysis and prediction of protein stability based on interaction network, gene ontology, and KEGG pathway enrichment scores. Biochim Biophys Acta Proteins Proteom. 2023;1871:140889. https://doi.org/10.1016/j.bbapap.2023.140889
23. Piñero J, Saüch J, Sanz F, Furlong LI. The DisGeNET cytoscape app: Exploring and visualizing disease genomics data. Comput Struct Biotechnol J. 2021;19:2960-7. https://doi.org/10.1016/j.csbj.2021.05.015
24. Gummagol NB, Yaraguppi DA, Patil SB, Patil PS, Patil NR, Ayachit NH. Exploring the anticancer potential of novel chalcone derivatives: Synthesis, characterization, computational analysis, and biological evaluation against breast cancer. J Mol Struct. 2025;1320:139586. https://doi.org/10.1016/j.molstruc.2024.139586
25. Hebasur RK, Koppal VV, Yaraguppi DA, Gummagol NB, Kusanur R, Patil NR. A comprehensive evaluation of a chalcone derivative: Structural, spectroscopic, computational, electrochemical, and pharmacological perspectives. Photochem. 2025;5(3):20. https://doi.org/10.3390/photochem5030020
26. Sehgal R, Sharma AK, Singh BJ, Saini RV, Saini AK, Beniwal V. Augmenting the antioxidant, anti-bacterial and anti-carcinogenic potential of *Terminalia chebula* and *Terminalia bellirica* after tannin acyl hydrolase mediated biotransformation. Biocatal Agric Biotechnol. 2024;56:103045. https://doi.org/10.1016/j.bcab.2024.103045
27. Mane R, Yaraguppi DA, Chandrakala KB, Kamanna K. Synthesis, computational, anticancer, and electrochemical behavior studies of 3-methyl-4-(hetero)arylmethyleneisoxazole-5(4h)-one. ChemistrySelect. 2024;9:e202401158. https://doi.org/10.1002/slct.202401158
28. Wan H, Williams R, Doherty P, Williams DF. A study of the reproducibility of the MTT test. J Mater Sci Mater Med. 1994;5(3):154-9. https://doi.org/10.1007/bf00053336
29. Umesh Kanna S, Parthiban KT, Senthilraja K, Venkatesan S, Udhaya Nandhini D, Mohan Kumar S, *et al*. Genetic diversity and structure of *Terminalia bellirica* (gaertn. Roxb.) Population in India as revealed by genetic analysis. Plants (Basel). 2024;13:470. https://doi.org/10.3390/plants13040470
30. Srinivasan M, Gangurde A, Chandane AY, Tagalpallewar A, Pawar A, Baheti AM. Integrating network pharmacology and *in silico* analysis deciphers Withaferin-A's anti-breast cancer potential via hedgehog pathway and target network interplay. Br Bioinform. 2024;25:bbae032. https://doi.org/10.1093/bib/bbae032
31. Zemnou CT. Network pharmacology, molecular docking, and molecular dynamics simulation revealed the molecular targets and potential mechanism of *Nauclea latifolia* in the treatment of breast cancer. Chem Biodivers. 2024;22:e202402423. https://doi.org/10.1002/cbdv.202402423
32. Baothman OA, Islam MR. Exploring breast cancer treatment paradigms: Innovative design, molecular docking and dynamic

simulation of LOXL2 inhibitors. Mol Simul. 2024;50:631-43. https://doi.org/10.1080/08927022.2024.2333907

33. Yang Z, Wang Y, Huang S, Geng Y, Yang Z, Yang Z. Identification of potential anti-tumor targets and mechanisms of huachansu injection using network pharmacology and cytological experiments in breast cancer. PLoS One. 2024;19:e0303650. https://doi.org/10.1371/journal.pone.0303650
34. El Rhabori S, Alaqarbeh M, El Aissouq A, Bouachrine M, Chtita S, Khalil F. Design, 3D-QSAR, molecular docking, ADMET, molecular dynamics and MM-PBSA simulations for new anti-breast cancer agents. Chem Phys Impact. 2024;8:100455. https://doi.org/10.1016/j.chphi.2023.100455
35. Zochedh A, Chandran K, Priya M, Sultan AB, Kathiresan T. DFT simulation of berberine chloride with spectroscopic characterization - biological activity and molecular docking against breast cancer. Polycycl Aromat Compd. 2024;44:1556-80. https://doi.org/10.1080/10406638.2023.2201457
36. Patil PV, Nerlekar NA, Kuldeep AR, Patil PP, Dandge PB, Dongale TD, *et al*. *Terminalia bellirica* (Gaertn.) Roxb. Extract-mediated green synthesis of magnesium oxide nanoparticles for multifunctional applications. Plant Nano Biol. 2024;8:100069. https://doi.org/10.1016/j.plana.2024.100069
37. Venturelli S, Niessner H, Sinnberg T, Berger A, Burkard M, Urmann C, *et al*. 6- and 8-prenylnaringenin, novel natural histone deacetylase inhibitors found in hops, exert antitumor activity on melanoma cells. Cell Physiol Biochem. 2018;51(2):543-56. https://doi.org/10.1159/000495275

How to cite this article:
Gadade A, Pattanashetti L, Prasanth DSNBK, Halkavatagi SG, Bagewadi ZK, Yaraguppi DA, Hallikeri NS. Phytochemical analysis and anti-breast cancer effects of *Terminalia bellirica* on MDA-MB-231 breast cancer cells: An integrated *in silico* and *in vitro* studies. J Appl Biol Biotech 2026. Article in Press. http://doi.org/10.7324/JABB.2026.248972